The International Society of Precision Agriculture presents the
15th International Conference on Precision Agriculture
26–29 JUNE 2022
Minneapolis Marriott City Center | Minneapolis, Minnesota USA

Gamma-ray spectrometry to determine soil properties for soil mapping in precision agriculture

Jasper Dreyer[1]; George van Zijl[1]; Laurent Ameglio[2]

[1]North-West University, 11 Hoffman Street Potchefstroom 2531, South Africa (jasper.dreyer@nwu.ac.za);

[2]EXIGE, 2 Yuluma Close, Bangor 2234, New South Wales, Australia (laurent@exigesa.com)

A paper from the Proceedings of the
15th International Conference on Precision Agriculture
June 26-29, 2022
Minneapolis, Minnesota, United States

Abstract.

Soil maps are critical for various land use applications and form the basis for the successful implementation of precision agriculture in crop production. High-resolution soil data is now required in the management of sustainable land-use practices and traditional soil maps often fail to provide these data. There is currently a stronger demand to understand soil variation at a finer scale. The use of gamma-radiometric data in conjunction with other information such as digital elevation models (DEM) or aerial photos has become an important source of data for digital soil mapping. The objective of this study was to determine the extent to which aerial gamma-ray spectroscopy, can successfully and practically be used to accurately determine soil management zones and topsoil properties for precision agriculture in the South African context. Airborne gamma-ray data was correlated with topsoil properties and soil types from a grid soil survey. The SCORPAN approach in the digital soil mapping was used for the predictive modelling and mapping of the soil properties and soil types. The covariate data consist of spectral, terrain and gamma data. The different soil properties was modelled using the Cubist and Random Forests regression decision trees. To predict the spatial distribution of soil types, the Multinomial Logistic Regression (MNLR) classification model were used. In this study the gamma-ray data was successful in predicting the soil particle fractions of sand, silt and clay, as well as the soil carbon (C), calcium (Ca) and magnesium (Mg), and with the mapping of soil types. Gamma-ray data can be used to map soil properties and soil types accurately, with 50% of the conventional soil samples and observations. This is a saving in both time and money. More research need to be done in bigger areas in South Africa to test the concept in the majority of crop production areas.

Keywords.

Soil maps, airborne gamma-ray spectrometry, soil properties, precision agriculture, digital soil mapping.

1. Introduction

Low potential arable land consists about one third (⅓) of the total arable land of South Africa (Le Roux *et al*., 2016). This low potential arable land is located mainly in semi-arid areas, with water shortage being the main problem. A low and erratic rainfall pattern is the reason for the water shortage. Under these circumstances, knowing the soil's physical properties is increasingly important for the management of soil water for successful crop production (Hillel, 2004).

The use of precision agriculture has been addressed as one of the solutions to meet food security (Talebpour, *et al*., 2015). Precision agriculture involves different technologies combined to enhance production within agricultural systems by keeping record of uncertainties and variability. Precision agriculture's role in food security is higher production and sustainable quality increase (Gebbers & Adamchuk, 2010).

Soil maps are critical for various land use applications and form the basis for the successful implementation of precision agriculture in crop production. Soil maps are graphic representations to provide the spatial distribution of important soil physical and chemical properties to a farmer (Yaalon, 1989). The farmer uses this information to make critical management decisions for profitable and sustainable food production (Weil & Brady, 2017). High-resolution soil data is now required in the management of sustainable land-use practices and traditional soil maps often fail to provide these data (Tunstall, 1998). There is currently a stronger demand to understand soil variation at a finer scale (Rampant & Abuzar, 2004).

The current South African conventional method for determining the spatial distribution of the soils physical and chemical properties is a grid survey, which includes soil classification and the sampling of the top soil for chemical analysis (Fertasa, 2016). This way of determining the spatial distribution of the soil is labour intensive, slow and thus costly (Viscarra Rossel & McBratney, 1998; Schuler *et al*., 2010; Van der Klooster *et al*., 2011). The sampling and measurement density of this conventional method is relatively coarse and may not be adequate to reveal all the variation in the soil (McBratney *et al*., 2005).

Advances in the fields of digital soil mapping (McBratney *et al*., 2003) and remote sensing allows experts to create timeous and cost effective soil maps (Mulder *et al*., 2011; Heggemann *et al*., 2017).

The knowledge of gamma-radiometric data and how it relate to soil-forming materials has increased the value of gamma-ray spectrometry for the use in digital soil mapping (McBratney *et al*., 2003). The use of gamma-radiometric data in conjunction with other information such as digital elevation models (DEM) or aerial photos has become an important source of data for digital soil mapping (Cook *et al*., 1996).

The aim of this study is to determine the extent to which aerial gamma-ray spectroscopy, can successfully and practically be used to accurately determine soil management zones for precision agriculture and determine the top soil properties like, texture, organic carbon, pH and plant-available nutrients (Ca, Mg, K and P) in the South African context.

1.1 Soil properties well correlated to Gamma radiometrics

Literature show that there are a good and reliable correlation between soil texture and soil gamma radiation (Heggemann *et al*., 2017; Herrmann, 2015; Pätzold *et al*., 2020; Petersen *et al*., 2012; Pracilio *et al*., 2006; Priori *et al*., 2013; Priori *et al*., 2014; Rouze *et al*., 2017a; Rouze *et al*., 2017b; Taylor *et al*., 2002; Van Egmond *et al*., 2010). The reason for this is that radionuclides form part of the soil mineral structure (K in clay minerals), radionuclides is part of the ions on the adsorption complex (K, Th) of soils, or it can be blocked in oxide minerals (U in goethite) (Reinhardt & Herrmann, 2019).

Gamma-ray spectrometry have the potential to offer a cheaper and spatially more precise alternative than conventional sampling and analysis of plant available potassium (K). In precision

agriculture this could be of great advantage (Wong & Harper, 1999). The study of Pracilio *et al*. (2006) concludes that plant available potassium (K) can reliably be predicted by radiometrics. It had to be kept in mind that processed fertilizer have different isotopic ratios, this can influence the correlation between gamma radiometrics and plant available potassium (K) (Alhardi, 2013; Chauhan *et al*., 2013). Thus some literature show no correlation between plant available potassium (K) and gamma-ray data (Dierke & Werban, 2013; Pätzold *et al*., 2020; Reinhardt and Herrmann, 2019).

The relationship between gamma radiation and soil pH is difficult to establish, because soil pH can readily change in agricultural landscapes by different management practises. The determination of pH values is an indirect effect, if working with gamma-ray spectrometry (Bierwirth *et al*., 1996).

A positive correlation was found between organic carbon and radiometric data by Martz and De Jong (1990), but clay was the real emitter because the organic carbon was strongly bound by the clay-complexes.

1.2 Soil type mapping

The relative disparity of gamma-ray signatures allows to theoretically classify soil types. On a global scale it is not possible to relate one soil type to one quantitative gamma-ray signature, because different combinations of soil forming factors and processes can lead to the same soil type. With different soil types in an area it is capable and effective to do soil type mapping with *in situ* gamma-ray spectrometry (Reinhardt & Herrmann, 2017). Literature show that gamma data can be used in different ways to distinguish between soil types (Alomari *et al*., 2019; Beamish, 2013; Marchuk & Ostendorf 2009; Martelet *et al*., 2014; Sanusi *et al*., 2014; Schuler *et al*., 2011; Vanden Bygaart & Protz, 2001).

2. Materials and methods

2.1 Study site

The study site is a 48 ha large irrigated field by centre pivot in the northern Free State province of the Republic of South Africa, near the confluence of the Vaal and Mooi Rivers. It lies approximate 24 km south west of Potchefstroom. The coordinates is S 26°52’42” and E 26°56’45”.

The terrain morphological class of the area can be described as plains with low relief, lying at an average altitude of around 1 308 meters above sea level (Kruger, 1983). The area is flat with a terrace going down to the flood plain of the Vaal River.

The study area is characterised by two different parent materials. In the north east next to the Vaal River it is Quaternary flood plain alluvium and the rest is deep eolian sand (Smit, 1986) with Vaalian diabase as the underlying geology (Council for Geoscience, 2008).

The climate of the area is hot and moist in the summer, with cool to cold, dry winters. The annual rainfall is 560 mm, with 83% of the total falling between October and March. The summer temperature is high with maximums of 29.8 °C (January) and minimums of -0.3 °C (July) (Kotze & Lonergan, 1984). According to the Land Type data (Land Type Survey Staff, 1984) this study site is of the Bd 13d land type.

2.2 Airborne gamma-ray data collection

Airborne gamma-ray data was obtained during March 2017. A Medusa MS 4000 gamma-ray sensor with a caesium-iodide CsI scintillator crystal of size 10.16 cm x 10.16 cm x 40.64 cm or

4.2 litres was used (Medusa, 2021). The spectrometer was mounted on board a gyrocopter flown by the geophysical company by the name of GyroLAG. The flight height was 20 meters above ground level and the line spacing was 20 meters apart at a speed of 120 kilometres per hour.

2.3 Soil survey, sampling and laboratory analysis

A soil survey was done in September 2014, where soils were described and classified, according to the South African Soil Classification System (Soil Classification Working Group, 1991) and Soil Taxonomy (Soil Survey Staff, 2003) on a 1 ha grid (100 m x 100 m) to a depth of 2.1 m or shallower if a restricting layer is encountered, using a hand auger. Soil sampling was conducted in March 2017. A total of 48 points were sampled at the same point where the soil classification was done. At each point three soil samples were collected by hand-auguring to a depth of 20 cm. These three samples were taken within a 1 m^2 area and combined into one sample. The samples were air-dried, crushed and passed through a 2 mm sieve to separate gravel and soil. The soil samples were analysed in the laboratory for $pH_{(water)}$ (1:2.5 soil/water ratio), electrical conductivity (EC) (saturated paste), %C (loss of ignition), exchangeable cations (Ca, Mg, K, Na) (ammonium acetate), phosphorus (Bray 1), and the percentage sand, silt and clay (NASAWC, 1990). The total elemental content was also measured with a Thermo Scientific Niton XL3t portable XRF analyser.

2.4 Covariate data used in study

The SCORPAN approach of McBratney *et al*. (2003) is used for the predictive modelling and mapping of the soil properties and soil types. The SCORPAN factors or environmental covariates is used to predict the soil type or attribute.

The covariate data used was the Sentinel satellite imagery for 6 March 2017 to present active growing crop and 13 August 2017 to present the bare soil (USGS, 2022) and the SRTM 30 m DEM (USGS, 2022). These vector data were rasterized and resampled to fit on the 10 m resolution grid of the Sentinel images. Spectral covariates were developed from the Sentinel 2A satellite. The spectral bands (blue, green, red & NIR) and indices (brightness, coloration, redness & saturation indexes) is the same that Flynn *et al*. (2019) used. They were used to present the vegetation and soil in the SCORPAN method.

From the DEM the various terrain derivatives that were calculated are analytical hillshading, slope, aspect, plan curvature, profile curvature, convergence index, closed depressions, flow accumulation, topographic wetness index, LS factor, channel base level, vertical distance to channel network, valley depth and relative slope position. All the GIS related calculations and derivatives were done in SAGA-GIS. The soil point dataset were linked to the covariates and exported into a text file (.txt), forming the database of the environmental covariates.

2.5 Digital Soil Mapping (DSM) of soil properties

The different soil properties was modelled using the Cubist and Random Forests regression decision trees (Malone *et al*., 2017). The soil properties dataset was divided into a training and independent dataset, using a stratified random sampling design. Different training dataset was made up with 50% and 75% of the dataset points, with all the covariates, with only the gamma-ray data and with only the spectral and terrain covariates.

The different models with the combination of different percentages of training data with the different covariate combinations used, was validated by means of RMSE, bias, R^2 and concordance.

2.6 Multinomial Logistic Regression (MNLR) for soil type mapping

A digital soil mapping (DSM) approach was used to predict the different soil properties with terrain, spectral and gamma-ray covariates. To predict the spatial distribution of soil types, the Multinomial Logistic Regression (MNLR) classification model were used (Kempen *et al*., 2003; Malone *et al*., 2017). The soil observation dataset was divided into a training and independent dataset, using a stratified random sampling design. Different training dataset was made up with 50% and 75% of the dataset points, with all the covariates, with only the gamma-ray data and with only the spectral and terrain covariates.

The soil maps were evaluated by comparing the dataset points, in the different evaluation datasets, to the relevant soil maps. This was done with the one-pixel buffer method as used by Van Zijl *et al*. (2012). Evaluation of the soil maps was done on the calculated total evaluation point accuracy and the Kappa coefficient.

3. Results and Discussion

3.1 Soil survey and classification data

Soil classification and soil texture determination of the study area, revealed two distinct soil types/bodies in the study area that correlate with the parent material, as seen in Figure 4c.

The soils in the alluvium is mainly of the Tukulu soil form and a few of the Oakleaf soil form (Tu), according to the South African soil classification system (Soil classification working group, 1991). The A horizon have an apedal to weak structure and a sandy loam textural class, with an average silt and clay content of 25%. The B horizon have a weak to modereate structure and a loam textural class. The mineralogy of the top soil in the alluvium is 71% quartz and 27.7% albite (Na-Feldspar). These soils can be placed in the Inceptisol, soil order, with Aquepts (Tukulu) and Ustepts (Oakleaf) as the suborders in Soil Taxonomy (Soil Survey Staff, 2003).

On the deep eolian sand further away from the river, the dominant soil forms was Clovelly and Longlands, with a single Vilafontes, Constantia and Pinedene in between (Cv) (Soil classification working group, 1991). The textural class of the A and sub-soil horizons is sand with less than 7% silt and clay combined. The structure of these soil is single-grained. The mineralogy of the top soil in the eolian sand is 74.3% quartz and 23.8% feldspar. In Soil Taxonomy (Soil Survey Staff, 2003) these soils can be placed in the Entisols, soil order with Psamments as the suborder.

3.2 Descriptive statistics of soil data

The descriptive statistics of the different topsoil (0-20 cm) properties measured in the laboratory are given in Table 1. Soil pH and percentage carbon (C) are the two soil properties with the lowest standard deviation (SD) of 0.29 and 0.43 respectively. The highest standard deviation (SD) was found for exchangeable calcium (Ca) and the potassium (K) measured with the portable XRF. The skewness of the soil properties, clay percentage, sand percentage, carbon percentage, exchangeable calcium (Ca) and magnesium (Mg) and portable XRF potassium (K) and portable XRF uranium (U), range between -0.5 and 0.5 which is an indication that the data is fairly symmetrical (Oliver and Webster, 2014). The electrical conductivity (EC) of the soil with a skewness of 4.09, is an indication that the data is highly skewed (Oliver and Webster, 2014). For pH and XRF potassium (K), the coefficient of variation (CV) was relative small with values of 4.7% and 8.4%, indicating their distribution has a low variation relative to the mean. The percentage clay (CV = 57.6%), electrical conductivity (EC) (CV = 133.3%) and XRF uranium (U) (CV = 90.7%) had the highest coefficient of variation (CV), meaning they have a high variation relative to the mean.

Table 1: Descriptive statistics of the topsoil (0-20 cm) properties at the 48 sampling points.

Soil Properties	Mean	Median	Standard deviation (SD)	Minimum	Maximum	Skewness	Kurtosis	Coefficient of variation (CV)
Clay (%)	8.4	8.4	4.8	0.4	19.3	0.18	-0.56	57.6
Silt (%)	11.7	11.3	6.3	1.1	32.8	0.90	1.66	53.9
Sand (%)	80.0	79.4	10.6	50.0	96.1	-0.47	0.28	13.3
pH H_2O	6.25	6.27	0.29	5.34	6.90	-0.84	2.17	4.7
EC (mS/m)	72	48	96	29	560	4.09	17.21	133.3
C % (LOI)	0.88	1.03	0.43	0.18	1.69	-0.06	-1.13	49.5
Exch. Ca (mg/kg)	1 027.9	1 126.0	592.7	151.0	2 211.5	0.04	-1.23	57.7
Exch. Mg (mg/kg)	217.0	231.8	122.2	35.5	545.5	0.38	-0.06	56.3
Exch. K (mg/kg)	125.7	129.8	69.2	0.5	392.0	0.82	3.48	55.1
Exch. Na (mg/kg)	14.7	10.8	18.1	0.5	78.5	2.16	4.96	123.1
P (mg/kg)	59.2	58.5	22.2	17.6	127.4	0.64	1.07	37.5
XRF K (ppm)	12 254.5	12 319.8	1 024.7	9 416.2	14 160.2	-0.34	0.08	8.4
XRF Th (ppm)	6.1	6.3	2.8	0.0	11.1	-0.65	0.50	45.7
XRF U (ppm)	4.3	5.4	3.9	0.0	11.4	0.01	-1.59	90.7

3.3 Descriptive statistics of aerial sensed data

The descriptive statistics of the aerial sensed data is presented in Table 2. This includes the elevation and gamma-ray spectrometry data. The statistics of the top half show the data for the whole field (n = 4 762). For elevation the mean and median were nearly equivalent. The 11.7 metre difference between the minimum (1 298.9 m) and maximum (1 310.6 m) is an indication that there is a major topographical variation. The field can be described as a flat upper part with a steep terrace leading to a lower relative flat area. The mean and median values for the gamma-ray data for the two radioelements K and Th and the ratio's for the different elements is almost equivalent, with only a slight difference for U and total count (TC). The total count (TC) data is not skewed (TC = -0.57).

Table 2: Summary statistics of the aerial sensed data, including elevation (m) and gamma-ray spectrometry across the whole field (4 762) and at sampling sites (48).

	Elevation (m)	K (%)	Th (ppm)	U (ppm)	TC (cps)	K / Th	K / U	Th / K	Th / U	U / K	U / Th
n = 4 762											
Mean	1 305.1	7.0	14.2	6.9	951.0	0.5	1.2	2.0	2.4	1.0	0.5
Median	1 305.0	7.1	14.5	5.7	972.4	0.5	1.2	2.0	2.5	0.8	0.4
SD	2.13	0.32	0.65	3.07	95.15	0.01	0.36	0.05	0.74	0.55	0.26
Minimum	1 298.9	4.7	9.5	3.4	743.6	0.4	0.2	1.7	0.4	0.5	0.2
Maximum	1 310.6	7.3	15.2	27.2	1 109.3	0.6	2.1	2.3	4.3	5.8	2.6
Skewness	0.19	-2.53	-2.06	2.16	-0.57	0.71	-0.57	0.08	-0.58	2.94	2.70
CV	0.16	4.63	4.60	44.16	10.01	2.35	31.29	2.32	31.37	53.66	52.79
n = 48											
Mean	1 305.2	7.0	14.2	7.3	948.1	0.5	1.1	2.0	2.3	1.1	0.5

Median	1 305.1	7.1	14.5	5.8	964.9	0.5	1.2	2.0	2.5	0.8	0.4
SD	2.02	0.37	0.67	3.53	94.93	0.01	0.36	0.05	0.73	0.66	0.31
Minimum	1 301.3	5.2	11.3	4.3	765.2	0.5	0.2	2.0	0.5	0.6	0.3
Maximum	1 309.3	7.2	14.8	23.3	1 088.5	0.5	1.7	2.2	3.5	4.5	2.1
Skewness	0.09	-3.03	-2.37	2.54	-0.51	-0.75	-0.64	0.99	-0.61	3.43	3.11
CV	0.16	5.32	4.71	48.36	10.01	2.17	32.18	2.22	32.20	61.62	58.47

Note: SD – standard deviation; CV – coefficient of variation.

In the bottom part of Table 2, the descriptive statistics of the aerial sensed data at the sampling sites (n = 48) is showed. The descriptive statistics show that the data at the sampling sites and that collected across the whole field, is in general nearly the same. This is an indication that the sampling sites are a fair and reasonable representation of the data collected across the whole field.

3.4 Pearson's correlation of aerial sensed data

The Pearson's correlation coefficient (r) of the aerial sensed data can be seen in Table 3. The statistics in the top half is for the whole field (n = 4 762). Between the majority of the gamma-ray data there was a strong and significant correlation (P < 0.001). For the individual radioelements, the highest correlation was between Th and K (0.89) followed by Th and U (-0.88). The cross-correlation between elevation and all four channels of the gamma-ray spectrometry was strongly correlated. The strongest correlation with elevation was between total count (-0.70), followed by Th (-0.51).

Table 3: Pearson's correlation coefficient (r) of the aerial sensed data, including elevation (m) and gamma-ray spectrometry across the whole field (4 762) and at sampling sites (48).

	Elevation (m)	K (%)	Th (ppm)	U (ppm)	TC (cps)	K / Th	K / U	Th / K	Th / U	U / K	U / Th
n = 4 762											
Elevation	1.00										
K	-0.40***	1.00									
Th	-0.51***	0.89***	1.00								
U	0.46***	-0.87***	-0.88***	1.00							
TC	-0.70***	0.51***	0.62***	-0.59***	1.00						
K / Th	0.21***	0.25***	-0.22***	0.01	-0.21***	1.00					
K / U	-0.50***	0.78***	0.80***	-0.92***	0.66***	-0.03	1.00				
Th / K	-0.20***	-0.29***	0.19***	0.04**	0.19***	-0.99***	-0.01	1.00			
Th / U	-0.51***	0.77***	0.81***	-0.92***	0.67***	-0.07***	0.99***	0.04**	1.00		
U / K	0.43***	-0.91***	-0.89***	0.99***	-0.55***	-0.06***	-0.87***	0.10***	-0.87***	1.00	
U / Th	0.45***	-0.89***	-0.90***	0.99***	-0.57***	0.01	-0.88***	0.03	-0.89***	0.99***	1.00
n = 48											
Elevation	1.00										
K	-0.49***	1.00									
Th	-0.56***	0.92***	1.00								
U	0.50***	-0.90***	-0.89***	1.00							
TC	-0.67***	0.54***	0.68***	-0.58***	1.00						

K / Th	0.01	0.52***	0.15	-0.32*	-0.14	1.00					
K / U	-0.56***	0.76***	0.80***	-0.90***	0.69***	0.16	1.00				
Th / K	0.01	-0.54***	-0.18	0.35*	0.12	-0.99***	-0.19	1.00			
Th / U	-0.57***	0.75***	0.81***	-0.90***	0.71***	0.12	0.99***	-0.14	1.00		
U / K	0.46***	-0.93***	-0.90***	0.99***	-0.53***	-0.39**	-0.84***	0.42**	-0.84***	1.00	
U / Th	0.48***	-0.92***	-0.91***	0.99***	-0.56***	-0.34*	-0.86***	0.37**	-0.86***	0.99***	1.00

Note: * P < 0.05; ** P < 0.01; *** P < 0.001.

In the bottom half of Table 3 the Pearson's correlation coefficient (r) for the aerial sensed data only at the sampling sites (n = 48) is shown. Like the data for the whole field, there was a strong and significant correlation (P < 0.001) between the majorities of the gamma-ray data at the sampling sites. The data for the sampling sites show a reflection of the data at the whole field. For the individual radioelements, again the highest correlation was between Th and K (0.92). This is followed by the correlation between K and U (-0.90). The cross-correlation between elevation and all four channels of the gamma-ray spectrometry show the same tendency with a strong correlation. The strongest correlation with elevation was with total count (-0.67), followed by Th (-0.56).

3.5 Pearson's correlation of aerial sensed data with soil data

In Table 4 the Pearson's correlation coefficients between the topsoil (0 – 0.2 m) properties and the aerial sensed gamma-ray data and elevation is shown. The individual radioelements of the gamma-ray data significantly correlated with the topsoil particle size fractions of sand, silt and clay. The largest and statistically most significant (P < 0.001) correlation was between total count (TC) with clay (0.82) and sand (0.81). There was also a significant correlation between the individual radioelements with soil carbon (C) and the exchangeable nutrient elements calcium (Ca) and magnesium (Mg). Total count again (TC) gave the largest and most statistically significant (P < 0.001) correlations with C (0.76), Ca (0.77) and Mg (0.78). No significant correlation was found between the gamma-ray data with soil pH, EC and P.

Table 4: Pearson's correlation coefficient (*r*) between aerial sensed data, including elevation (m) and gamma-ray spectrometry and various topsoil (0 – 0.2 m) chemical and physical properties.

	C	Sand	Silt	Clay	Exchangeable		
	(%)	(%)	(%)	(%)	Ca (mg/kg)	Mg (mg/kg)	K (mg/kg)
Elevation (m)	-0.64***	0.56***	-0.46***	-0.63***	-0.63***	-0.60***	-0.35*
K (%)	0.56***	-0.54***	0.46***	0.58***	0.54***	0.52***	0.42**
Th (ppm)	0.60***	-0.58***	0.49***	0.63***	0.58***	0.56***	0.41**
U (ppm)	-0.61***	0.57***	-0.48***	-0.63***	-0.58***	-0.56***	-0.42**
TC (cps)	0.76***	-0.81***	0.73***	0.82***	0.77***	0.78***	0.38**
K / Th	0.09	-0.08	0.08	0.08	0.07	0.07	0.17
K / U	0.70***	-0.65***	0.56***	0.69***	0.68***	0.64***	0.43**
Th / K	-0.11	0.10	-0.09	-0.10	-0.09	-0.09	-0.18
Th / U	0.70***	-0.65***	0.56***	0.70***	0.68***	0.64***	0.42**
U / K	-0.56***	0.53***	-0.44**	-0.59***	-0.53***	-0.52***	-0.41**
U / Th	-0.58**	0.54***	-0.45**	-0.60***	-0.55***	-0.53***	-0.41**

Note: * P < 0.05; ** P < 0.01; *** P < 0.001.

3.6 Spatial distribution of aerial sensed data

The spatial distribution of the study field's elevation is shown in Figure 1. At the south western side of the field the elevation was the highest (1 310.6 m) with the lowest (1 298.9 m) point in the north western side. There is quite a steep fall in elevation from the south west to the north east, in the form a terrace. The site can be described as having an upper south western part and a lower north eastern part.

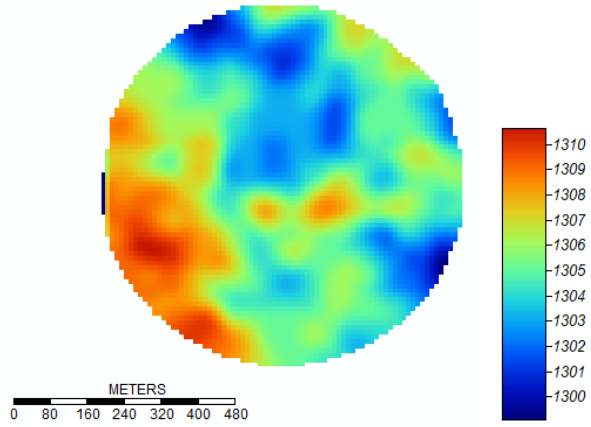

Figure 1: Spatial distribution of elevation data (m).

The gamma-ray data's spatial distribution is shown in Figure 2. In Figure 2a K(%) is shown, with the highest values (7.0-7.28 %) in the northern and eastern part covering the largest area. Intermediate K values (6.38-6.60 ppm) is found in the south western part with some spots in the eastern part. Thorium in Figure 2b follow the same trend as K, with the spatial distribution of U in Figure 2c with an inverse trend of K and Th. Total count as shown in Figure 2d have the lowest (760-840 cps) count in the south western part with the highest (1 000-1 100 cps) count running in the centre from north to south.

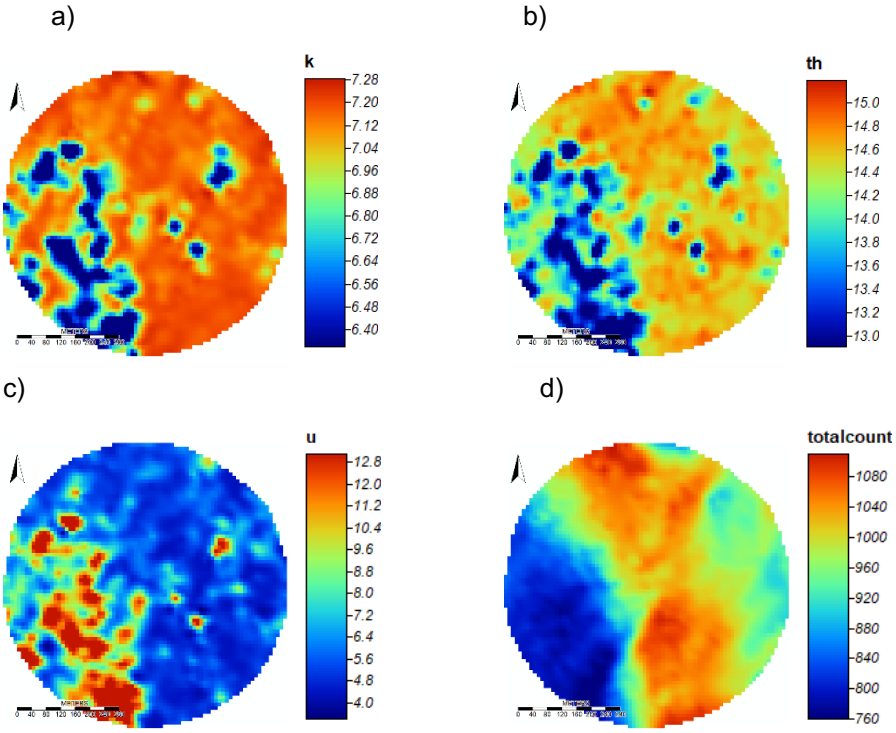

Figure 2: Spatial distribution of interpolated gamma-ray spectrometry data for a) potassium (K - %), b) thorium (Th – ppm), c) uranium (U – ppm) and total counts (TC – cps).

3.7 Spatial distribution of soil properties

The spatial distribution of the various topsoil (0-0.2 m) properties is shown in Figure 3. The carbon content is shown in Figure 3a, with the lowest carbon content of 0.6% and less in the western half of the field. Figure 3b shows the clay percentage, with the highest clay (12-16%) in the northern and south eastern part of the field. The lowest clay (0-7%) was in the western part of the field. Figures 3c to 3e shows the Ca, Mg and K maps. The highest amounts of these element is found in the northern and south eastern parts of the field, with the lowest amounts in the western part of the field. The carbon, calcium, magnesium and potassium maps show the same tendency than the clay map, with the higher C, Ca, Mg and K correlated with the higher clay content. The amount of these elements is thus a function of the clay content of the soil (Weil & Brady, 2017).

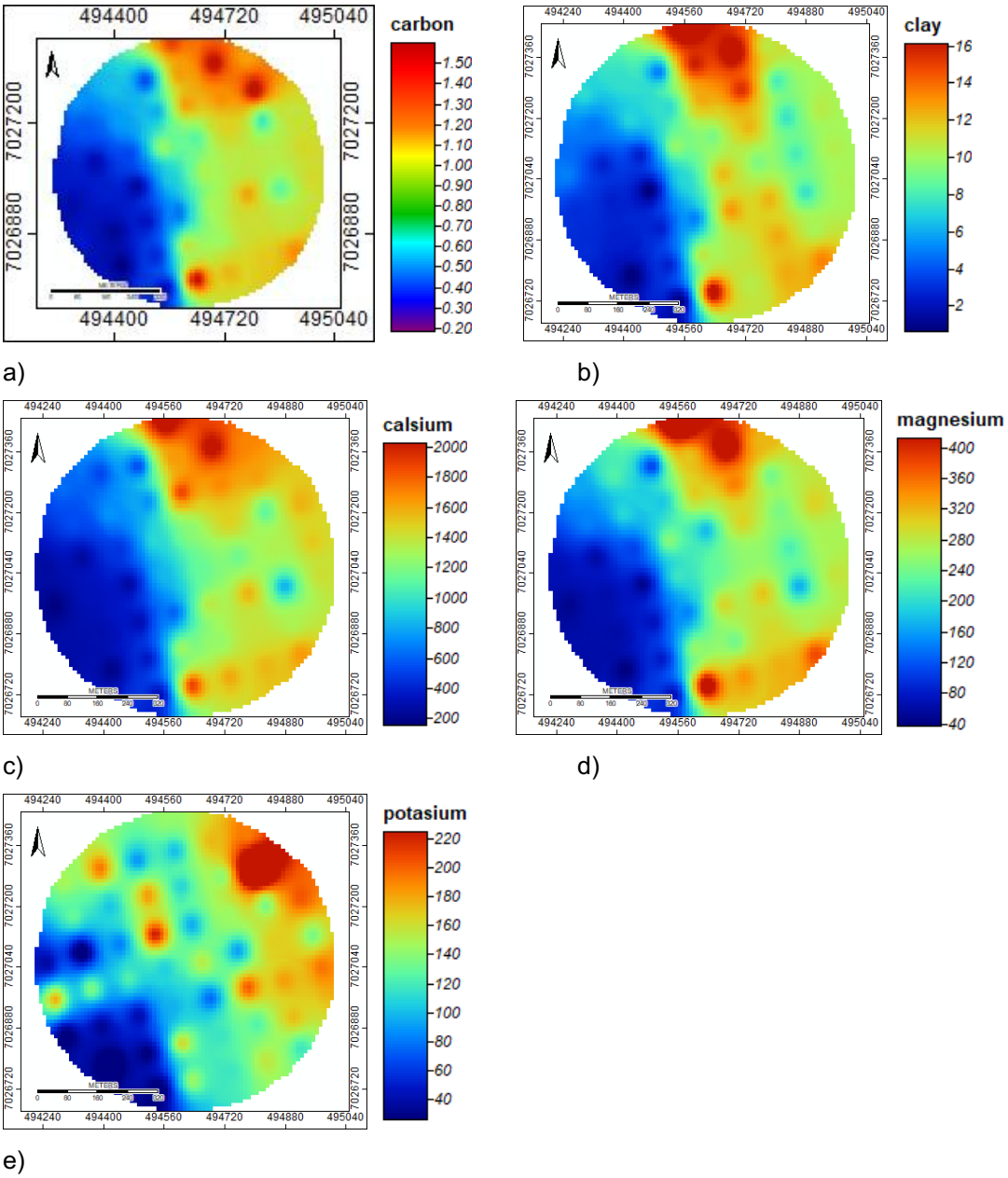

Figure 3: Spatial distribution of interpolated topsoil (0-0.2 m) a) carbon (%), b) clay (%), c) Ca (mg/kg), d) Mg (mg/kg) and e) K (mg/kg).

3.8 Spatial soil property mapping with Digital Soil mapping methods

Table 5 gives a comparison of results between the Cubist and Random Forest models for a

calibration with 50% (24 samples) and 75% (36 samples) of the data. The soil properties with coefficient of determination (R^2) and concordance values of 0.5 and higher are, carbon (C), sand, silt, clay, calcium (Ca) and magnesium (Mg). For these soil properties, the gamma-ray covariates alone gives by far better values than the terrain and spectral covariates alone. The comparison between gamma-ray covariates alone and all the covariates together, the combination of all the covariates gave an equal or slight better value. For carbon (C) with the cubist model, the gamma-ray covariates alone gave even higher values than the combination of all the covariates together. The gamma-ray data thus predict the above soil properties by far better than the terrain and spectral data.

Table 5: Comparison between the Cubist and Random Forest models for the Digital Soil Mapping (DSM) of the soil properties with Terrain and Spectral covariates, Gamma-ray covariates and the combination of both. The modelling was done with 50% (24 samples) and 75% (36 samples) of the data for calibration.

Soil property	Model	Quality measures	Terrain and Spectral		Gamma-ray		All data	
			50%	75%	50%	75%	50%	75%
C	Cubist	R^2	0.42	-0.08	0.59	0.66	0.09	0.30
		Concordance	0.62	0.10	0.71	0.73	0.35	0.55
	Random Forest	R^2	0.52	0.14	0.61	0.80	0.76	0.18
		Concordance	0.63	0.29	0.72	0.82	0.76	0.41
Sand	Cubist	R^2	0.09	0.12	0.64	0.59	0.64	0.40
		Concordance	0.34	0.41	0.76	0.68	0.76	0.59
	Random Forest	R^2	0.29	0.11	0.45	0.55	0.28	0.65
		Concordance	0.53	0.27	0.64	0.67	0.45	0.69
Silt	Cubist	R^2	0.27	0.19	0.28	0.40	0.29	0.59
		Concordance	0.52	0.40	0.45	0.59	0.46	0.59
	Random Forest	R^2	0.16	0.50	0.23	0.54	0.50	0.72
		Concordance	0.37	0.55	0.40	0.60	0.53	0.64
Clay	Cubist	R^2	0.32	0.42	0.67	0.57	0.61	0.74
		Concordance	0.53	0.61	0.78	0.65	0.70	0.80
	Random Forest	R^2	0.40	0.03	0.61	0.53	0.64	0.68
		Concordance	0.59	0.21	0.68	0.69	0.60	0.74
Ca	Cubist	R^2	0.34	0.47	0.59	0.81	0.69	0.33
		Concordance	0.58	0.66	0.71	0.82	0.76	0.43
	Random Forest	R^2	0.44	0.08	0.55	0.32	0.67	0.46
		Concordance	0.60	0.35	0.71	0.55	0.73	0.54
Mg	Cubist	R^2	0.04	0.55	0.62	0.67	0.09	0.38
		Concordance	0.26	0.68	0.72	0.72	0.32	0.59
	Random Forest	R^2	0.18	0.63	0.32	0.61	0.56	0.53
		Concordance	0.39	0.73	0.53	0.70	0.63	0.63

3.9 Soil type mapping with Multinomial Logistic Regression (MNLR)

Table 6 shows the comparison of the accuracy and Kappa coefficients for the predictions obtained with the Multinominal Logistic Regression (MNLR) machine learning algorithm for the validation data. This is for all the covariate data, gamma-ray data and terrain and spectral covariate data, with 50% and 75% as training dataset.

Table 6: Comparison of the accuracy and Kappa values for the predictions of the validation data.

Covariate data		Accuracy (%)	Kappa coefficient	Number of mapping units
All	75%	67	0.41	3
	50%	71	0.42	2
Gamma	75%	92	0.81	3
	50%	96	0.89	3
Terrain & Spectral	75%	67	0.45	3
	50%	55	0.28	3

The best accuracy (92% and 96%) and Kappa coefficients (0.81 and 0.89) was obtained with the gamma-ray covariate data alone. The other covariate data used gave accuracies from 55% to 71% and Kappa coefficients of 0.28 to 0.45. According to Landis and Koch (1977), the Kappa coefficients of the gamma-ray data can be interpreted as an almost perfect agreement, while the rest is a fair to moderate agreement. The gamma-ray data thus map the soil types better than all the data used together and the terrain and spectral data used alone. Figure 4 show the soil maps obtained from the gamma-ray covariate data (4a and 4b) with the Multinominal Logistic Regression (MNLR) machine learning algorithm compared to the traditional soil map (4c).

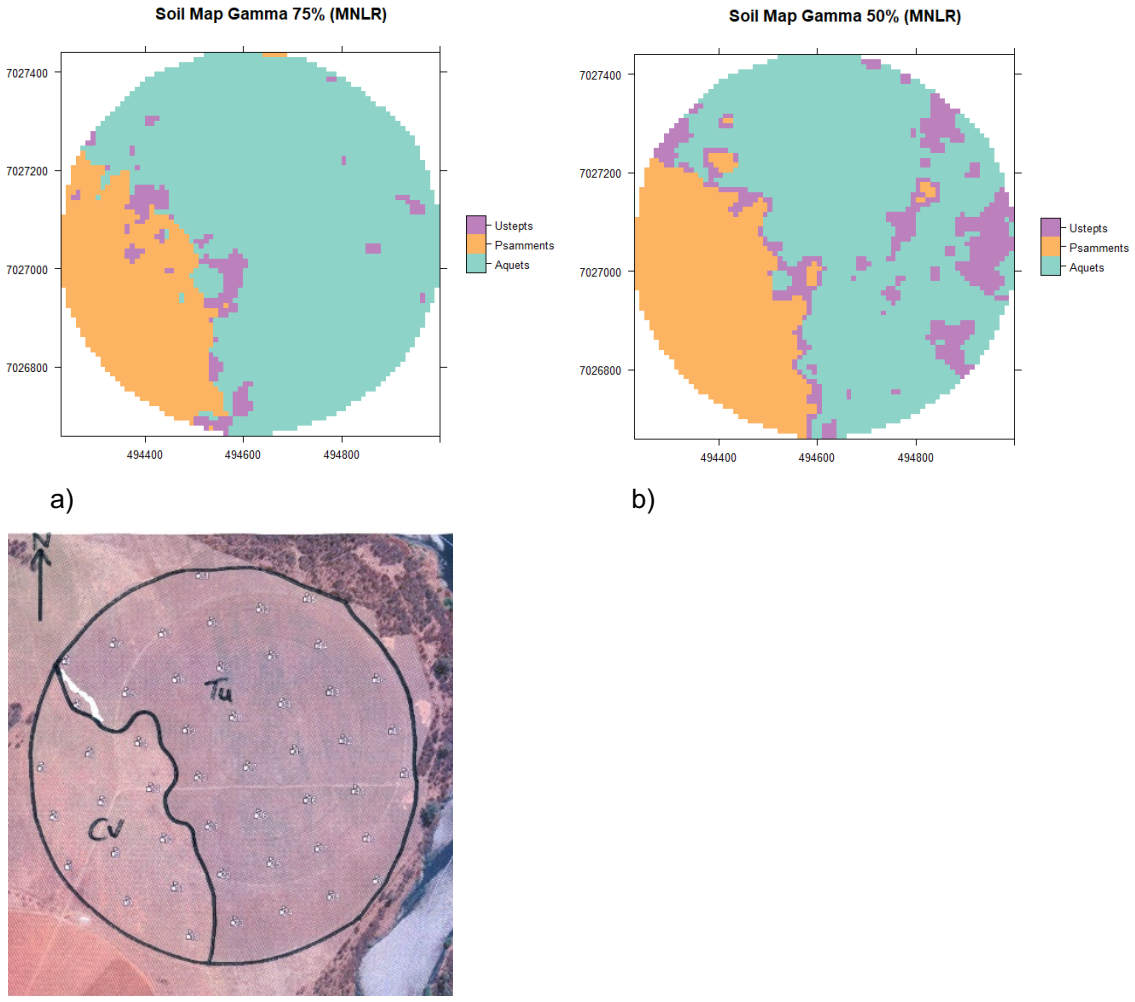

Figure 4: Soil type maps of a) gamma 75% training data, b) gamma 50% training data and c) traditional soil map.

4. Conclusions

The digital soil mapping results (Table 5) and the results of the Pearson's correlation of the aerial gamma-ray sensed with the soil properties (Table 4), show the same results. With both, the gamma-ray data correlate with soil carbon (C), sand, silt, clay, calcium (Ca) and magnesium (Mg). Since the gamma-ray data is a reflection of the soil mineralogy, the soil textural fractions is predicted by the gamma-ray data. The soil carbon (C), calcium (Ca) and magnesium (Mg) is a function of the clay content of the soil. This conclude that aerial sensed gamma-ray spectrometry data can successfully be used to directly estimate and predict the soil textural properties and indirectly the soil chemical properties that is related to the soil texture. Thus gamma-ray spectroscopy improve and can successfully be used to map soil properties for precision agriculture. This is proof from the correlations between the gamma data and soil properties.

The use of gamma-ray data in digital soil mapping for soil type maps proves to be far better than the terrain and spectral data for soil type mapping. With gamma data, zones of soil types can be better mapped than conventional soil type mapping.

In this study the gamma-ray data was successful in predicting the soil particle fractions of sand, silt and clay, as well as the soil carbon (C), calcium (Ca) and magnesium (Mg), and with the mapping of soil types. Gamma-ray data can be used to map soil properties and soil types accurately, with 50% of the conventional soil samples and observations. This is a saving in both time and money. More research need to be done in bigger areas in South Africa to test the concept in the majority of crop production areas.

References

Alharbi, W.R. 2013. Natural radioactivity and dose assessment for brands of chemical and organic fertilizers used in Saudi Arabia. *Journal of Modern Physics*, 4(3):344-348.

Alomari, A.H., Saleh, M.A., Hashim, S. & Alsayaheen, A. 2019. Investigation of natural gamma radiation dose rate (GDR) levels and its relationship with soil type and underlying geological formations in Jordan. *Journal of African Earth Sciences*, 155:32-42.

Beamish, D. 2013. Gamma-ray attenuation in the soils of Northern Ireland, with special reference to peat. *Journal of Environmental Radioactivity*, 115:13-27.

Bierwirth, P., Gessler, P. & McKane, D. 1996. Empirical investigation of airborne gamma-ray images as an indicator of soil properties-Wagga Wagga, NSW. In: 8th Australian Remote Sensing Conference Proceedings, March 25 – 29, 1996, Canberra, Australia, pp. 320-327.

Chauhan, P., Chauhan, R.P. & Gupta, M. 2013. Estimation of naturally occurring radionuclides in fertilizers using gamma-ray spectrometry and elemental analysis by XRF and XRD techniques. *Microchemical Journal*, 106:73-78.

Cook, S.E., Corner, R.J., Groves, P.R. & Grealish, G.J. 1996. Use of airborne gamma radiometric data for soil mapping. *Australian Journal of Soil Research*, 34(1):183-194.

Council for Geoscience. 2008. Simplified geological map of the Republic of South Africa and the Kingdoms of Lesotho and Swaziland. 1: 2 000 000. Council for Geoscience. Pretoria.

Dierke, C. & Werban, U. 2013. Relationships between gamma-ray data and soil properties at an agricultural test site. *Geoderma*, 199:90-98.

Fertasa (Fertilizer Association of Southern Africa). 2016. *Fertilizer Handbook*. 8th ed. Pretoria: Fertasa.

Flynn, T., Van Zijl, G.M., Van Tol, J.J., Botha, C.C., Rozanov, A., Warr, B. & Clarke, C. 2019. Comparing algorithms to disaggregate complex soil polygons in contrasting environments. *Geoderma*, 352:171-180.

Gebbers, R. & Adamchuk, V.I. 2010. Precision agriculture and food security. *Science*, 327(5967):828-831.

Heggemann, T., Welp, G., Amelung, W., Angst, G., Franz, S.O., Koszinski, S., Schmidt, K. & Pätzold, S. 2017. Proximal gamma-ray spectrometry for site-independent in situ prediction of soil texture on ten heterogeneous fields in Germany using support vector machines. *Soil and Tillage Research*, 168:99-109.

Herrmann, L. 2015. Scales in soil science. Aspects and prospects. Habilitation treatise, University of Hohenheim, Germany.
Hillel, D. 2004. *Introduction to Environmental Soil Physics*. Burlington, MA: Elsevier.
Kempen,B., Brus, D.J., Heuvelink, G.B.M. & Stoorvogel, J.J. 2009. Updating the 1:50 000 Dutch soil map using legacy soil data: a multinomial logistic regression approach. *Geoderma*, 151:311-326.
Kotze, A.V. & Lonergan, A.T. 1984. Climate data. In: *Land types of the maps 2626 West Rand and 2726 Kroonstad. Mem. Agric. nat. Resour. .S.Afr*. No.4. Department of Agriculture, Pretoria.
Kruger, G.P. 1983. Terrain Morphological Map of Southern Africa. Department of Agriculture. Pretoria.
Landis, R. & Koch, G.G. 1977. The measurement of observer agreement for categorical data. *Biometrics*, 33:159-174.
Land Type Survey Staff. 1984. Land types of the maps 2626 Wes-Rand, 2726 Kroonstad. *Memoirs on the Agricultural Natural Resources of South Africa*. No. 4.
Le Roux, P.A.L., Hensley, M., Van Rensburg, L.D. & Botha, J.J. 2016. The cropping potential of South Africa: land evaluation results obtained during the last 50 years. *South African Journal of Plant and Soil*, 33(2):83–88.
Malone, B.P., Minasny, B. & McBratney, A.B. 2017. Using R for digital soil mapping. Switzerland: Springer.
Marchuk, S. & Ostendorf, B. 2009. Relationship between soil properties and airborne gamma-radiometric data. In: Ostendorf, B., Baldock, P., Bruce, D., Burdette, M. & Corcoran, P. eds. *Proceedings of the Surveying & Spatial Sciences Institute Biennial International Conference*. Adelaide, Australia: Surveying & Spatial Sciences Institute. pp. 1041-1051.
Martelet, G., Nehlig, P., Arrouays, D., Messner, F., Tourlière, B., Laroche, B., Deparis, J., Saby, N.P.A., Richer de Forges, A., Jolivet, C. & Ratié, C. 2014. Airborne Gamma-Ray Spectrometry: Potential for Regolith-Soil Mapping and Characterization. In: Arrouays, D., McKenzie, N., Hempel, J., Richer de Forges, A. & McBratney, A.B., eds. *Global Soil Map: Basis of the global spatial soil information system*. Boca Raton, FL: CRC Press. pp. 401-408.
Martz, L.W. & De Jong, E. 1990. Natural radionuclides in the soils of a small agricultural basin in the Canadian prairies and their association with topography, soil properties and erosion. *Catena*, 17:85-69.
McBratney, A.B., Santos, M.M.L. & Minasny, B. 2003. On digital soil mapping. *Geoderma*, 117:3-52.
McBratney, A.B., Whelan, B., Ancev, T. & Bouma, J. 2005. Future directions of precision agriculture. *Precision Agriculture*, 6(1):7-23.
Medusa. 2021. *Medusa Products*. https://medusa-online.com/en/products/sensors/ Date of access: 3 March 2021.
Mulder, V.L., De Bruin, S., Schaepman, M.E. & Mayr, T.R. 2011. The use of remote sensing in soil and terrain mapping – A review. *Geoderma*, 162:1-19.
NASAWC (Non-Affiliated Soil Analysis Working Committee). 1990. *Handbook of standard soil testing methods for advisory purposes*. Pretoria: Soil Science Society of South Africa.
Oliver, M.A. & Webster, R. 2014. A tutorial guide to geostatistics: Computing and modelling variograms and kriging. *Catena*, 113:56-69.
Pätzold, S., Leenen, M. & Heggemann, T.W. 2020. Proximal mobile gamma spectrometry as tool for precision farming and field experimentation. *Soil systems*, 4(2):1-23.
Petersen, H., Wunderlich, T., Attia al Hagrey, S. & Rabbel, W. 2012. Characterization of some Middle European soil textures by gamma-spectrometry. *Journal of Plant Nutrition and Soil Science*, 175(5):651-660.
Pracilio, G., Adams, M.L., Smettem, K.R.J. & Harper, R.J. 2006. Determination of spatial distribution patterns of clay and plant available potassium contents in surface soils at the farm scale using high resolution gamma ray spectrometry. *Plant and Soil*, 282:67-82.
Priori, S., Bianconi, N., Fantappiè, M., Guaitoli, F., Pellegrin, S., Ferrigno, G. & Costantini, E.A.C. 2013. The potential of gamma-ray spectroscopy for soil proximal survey in clayey soils. *Journal of Environmental Quality*, 11:29-38.
Priori, S., Bianconi, N. & Costantini, E.A.C. 2014. Can γ-radiometrics predict soil textural data

and stoniness in different parent materials? A comparison of two machine-learning methods. *Geoderma*, 226:354-364.
Rampant, P. & Abuzar, M. 2004. Geophysical tools and digital elevation models: Tools for understanding crop yield and soil variability. *SuperSoil 2004: 3rd Australian New Zealand Soils Conference.* CDROM, www.regional.org.au/au/asssi/.
Reinhard, N. & Herrmann, L. 2017. Fusion of indigenous knowledge and gamma spectrometry for soil mapping to support knowledge-based extension in Tanzania. *Food Security*, 9(6):1271-1284.
Reinhard, N. & Herrmann, L. 2019. Gamma-ray spectrometry as versatile tool in soil science: a critical review. *Journal of Plant nutrition and Soil science*, 182:9-27.
Rouze, G.S., Morgan, C.L.S., McBratney, A.B. & Neely, H.L. 2017a. Exploratory assessment of United States aerial gamma radiometrics. *Soil Science Society of America Journal*, 81(1):94-108.
Rouze, G.S., Morgan, C.L.S. & McBratney, A.B. 2017b. Understanding the utility of aerial gamma radiometrics for mapping soil properties through proximal gamma surveys. *Geoderma*, 289:185-195.
Sanusi, M.S.M., Ramli, A.T., Gabdo, H.T., Garba, N.N., Heryanshah, A., Wagiran, H. & Said, M.N. 2014. Isodose mapping of terrestrial gamma radiation dose rate of Selangor state, Kuala Lumpur and Putrajaya, Malaysia. *Journal of environmental radioactivity*, 135:67-74.
Schuler, U., Herrmann, L., Ingwersen, J., Erbe, P. & Stahr, K. 2010. Comparing mapping approaches at subcatchment scale in northern Thailand with emphasis on the maximum likelihood approach. *Catena*, 81(2):137-171.
Schuler, U., Erbe, P., Zarei, M., Rangubpit, W., Surinkum, A., Stahr, K. & Herrmann, L. 2011. A gamma-ray spectrometry approach to field separation of illuviation-type WRB reference soil groups in Northern Thailand. *Journal of Plant nutrition and Soil science*, 174:536-544.
Smit, P.J. 1986. *2626 West Rand 1:250 000 geological map*. Department of mineral and energy affairs. Pretoria.
Soil Classification Working Group. 1991. *Soil classification – A taxonomic system for South Africa*. Memoirs on the South African Natural Resources No. 15. Department of Agricultural Development. Pretoria.
Soil Survey Staff. 2003. Keys to Soil Taxonomy. 9th Edition. United States Department of Agriculture, Natural Resources Conservation Service. U.S. Government Printing Office. Washington DC. 20402.
Talebpour, B., Türker, U. & Yegül, U. 2015. The role of precision agriculture in the promotion of food security. *International Journal of Agricultural and Food Research*, 4(1):1-23.
Taylor, M.J., Smettem, K., Pracilio, G. & Verboom, W. 2002. Relationships between soil properties and high-resolution radiometrics, central eastern Wheatbelt, Western Australia. *Exploration Geophysics*, 33(2):95-102.
Tunstall, B. 1998. Application of radiometrics to soil survey: Some basic consideration. *Australian Collaborative Land Program Newsletter*, 7(2):28-31.
USGS. 2022. https://earthexplorer.usgs.gov/ Date of access: 14 Feb. 2022.
Van der Klooster, E., Van Egmond, F.M. & Sonneveld, M.P.W. 2011. Mapping soil clay contents in Dutch marine districts using gamma-ray spectrometry. *European Journal of Soil Science*, 62(5):743-753.
Van Egmond, F.M., Loonstra, E.H. & Limburg, J. 2010. Gamma-ray sensor for topsoil mapping: The Mole. In: Viscarra Rossel, R.A., McBratney, A.B. & Minasny, B., eds. *Proximal Soil Sensing*. Dordrecht: Springer. pp. 323-332.
Van Zijl, G.M., Le Roux, P.A.L. & Smith, H.J.C. 2012. Rapid soil mapping under restrictive conditions in Tete, Mozambique. In: Minasny, B., Malone, B.P. & McBratney, A.B., eds. *Digital soil assessments and beyond*. Boca Raton, FL: CRC Press. pp. 335-339.
Vanden Bygaart, J. & Protz, R. 2001. Bomb-fallout 137Cs as a marker of geomorphic stability in dune sands and soils, Pinery Provincial Park, Ontario Canada. *Earth Surface Processes and Landforms*, 26(6):689-700.
Vicarra Rossel, R.A. & McBratney, A.B. 1998. Soil chemical analytical accuracy and costs: implications from precision agriculture. *Australian Journal of Experimental Agriculture*, 38:765-

775.
Weil, R.R. & Brady, N.C. 2017. *The nature and properties of soils*. 15th ed. Harlow: Pearson.
Wong, M.T.F. & Harper, R.J. 1999. Use of on-ground gamma-ray spectrometry to measure plant-available potassium and other topsoil attributes. *Australian Journal of Soil Research*, 37(2):267-278.
Yaalon. D.H. 1989. The earliest soil maps and their logic. *Bulletin of the International Society of Soil Science*. *International Society of Soil Science, Wageningen*, 24.